Lateral migration patterns toward or away from injection wells for earthquake clusters in Oklahoma

José-Ángel López-Comino[1], martin galis[2], P. Martin Mai[3], Xiaowei Chen[4], and Daniel Stich[5]

[1]KAUST, King Abdullah University of Science and Technology
[2]KAUST
[3]King Abdullah University of Science & Technology
[4]University of Oklahoma
[5]Universidad de Granada

November 24, 2022

Abstract

Exploring the connections between injection wells and seismic migration patterns is key to understanding processes controlling growth of fluid-injection induced seismicity. Numerous seismic clusters in Oklahoma have been associated with wastewater disposal operations, providing a unique opportunity to investigate migration directions of each cluster with respect to the injection-well locations. We introduce new directivity migration parameters to identify and quantify lateral migration toward or away from the injection wells. We take into account cumulative volume and injection rate from multiple injection wells. Our results suggest a relationship between migration patterns and the cluster-well distances, and unclear relationship with injected volume and equivalent magnitudes. Migration away from injection wells is found for distances shorter than 5-13 km, while an opposite migration towards the wells is observed for larger distances, suggesting an increasing influence of poroelastic stress changes. This finding is more stable when considering cumulative injected volume instead of injection rate.

Lateral migration patterns toward or away from injection wells for earthquake clusters in Oklahoma

J. A. López-Comino[1,2,3,4], M. Galis[5,6], P. M. Mai[1], X. Chen[7] , D. Stich[2,3]

[1] KAUST, King Abdullah University of Science and Technology, Thuwal (Saudi Arabia).

[2] Instituto Andaluz de Geofísica, Universidad de Granada, Granada, Spain.

[3] Departamento de Física Teórica y del Cosmos, Universidad de Granada, Granada, Spain.

[4] Institute of Earth and Environmental Sciences, University of Potsdam, D-14476 Potsdam-Golm, Germany

[5] Faculty of Mathematics, Physics and Informatics, Comenius University in Bratislava, Slovakia

[6] Earth Science Institute, Slovak Academy of Sciences, Bratislava, Slovakia

[7] School of Geosciences, The University of Oklahoma, Norman, OK, USA

Corresponding author: José Ángel López-Comino (jose.lopezcomino@kaust.edu.sa)

Key Points (140 characters)

- We introduce new parameters to analyze lateral seismicity migration patterns toward or away from multiple associated fluid-injection wells
- Cluster-well distance appears as the main factor in migration behavior in comparison with injected volumes or equivalent magnitudes
- Migration away from injection wells is found for distances shorter than 5-13 km, migration toward the wells at larger distances

Abstract (150 words)

Exploring the connections between injection wells and seismic migration patterns is key to understanding processes controlling growth of fluid-injection induced seismicity. Numerous seismic clusters in Oklahoma have been associated with wastewater disposal operations, providing a unique opportunity to investigate migration directions of each cluster with respect to the injection-well locations. We introduce new directivity migration parameters to identify and quantify lateral migration toward or away from the injection wells. We take into account cumulative volume and injection rate from multiple injection wells. Our results suggest a relationship between migration patterns and the cluster-well distances, and unclear relationship with injected volume and equivalent magnitudes. Migration away from injection wells is found for distances shorter than 5-13 km, while an opposite migration towards the wells is observed for larger distances, suggesting an increasing influence of poroelastic stress changes. This finding is more stable when considering cumulative injected volume instead of injection rate.

Plain Language Summary

Oklahoma seismicity has been linked to wastewater injection and provides one of the most important datasets to explore connections between injection wells and induced seismicity. This induced seismicity can be associated in different groups (or clusters) that reveal specific spatiotemporal relationships from which preferred spatial migration directions can be identified. We analyzed seismic migration directions of these clusters with the aim of understanding the growth of the rupture process and its location with respect to the closest injection wells. We introduce new techniques and parameters to quantify lateral migration patterns toward or away from injection-well locations. Different variables such as the cluster-well distance, injected volumes and magnitudes are considered to assess their influence in these migration behaviors. We identify the main pattern depending on the cluster-well distances. At shorter distances (up to 13 km), we observe dominantly migration away from injection wells (particularly for distances shorter than 5 km), whereas at larger distances we observe migration toward the wells.

1 Introduction

In the last decade, seismic activity observed in Oklahoma has attracted considerable public attention because the annual rate of earthquakes increased since 2009 due to wastewater injection (Ellsworth, 2013; Weingarten et al., 2015; Hincks et al., 2018). Exploring spatio-temporal relations between injection wells and seismic migration patterns is key to understanding the processes controlling the growth of injection-induced seismicity. Earthquakes tend to migrate away from the fluid source following the diffusion of pore pressure, from which hydraulic diffusivity properties can be modeled (Shapiro et al., 2005). However, plausible lateral migration patterns toward or away from injection wells in large-scale fluid-injection stimulated areas such as Oklahoma remain unclear (Haffener et al., 2018). Yet, if lateral migration patterns exist and can be tied to (controllable) injection processes, important implications for (time-dependent) fluid-induced seismic hazard assessment arise. This study investigates such properties through a comprehensive migration analysis with respect to multiple injection wells for the Oklahoma seismic clusters. These clusters are defined by applying clustering techniques that associate seismic events into specific groups (or clusters) with specific spatiotemporal relationships, deciphering also different fault structures (Ester et al., 1996; Wang et al., 2013; Zaliapin and Ben-Zion, 2013; Cheng and Chen, 2018). The identification and characterization of these clusters has been well studied in natural and tectonic contexts revealing interesting event migration features such as, for instance, event triggering due to fluid flow (Vidale and Shearer, 2006; Chen et al., 2012; Passarelli et al., 2018).

Recent efforts for improving the existing earthquake catalogues for Oklahoma identified seismicity clusters distributed over the area due to the activation of hundreds of previously unknown faults (Schoenball and Ellsworth, 2017). Analyzing the spatiotemporal evolution of these clusters reveals that seismicity tends to initiate at shallower depth and migrates deeper along faults as the sequence proceeds (Schoenball and Ellsworth, 2017b). Although 40 – 50% of individual clusters exhibit statistically significant diffusive migration, no clear migration patterns along-strike are observed (Haffener et al., 2018). On the other hand, preferred rupture propagation direction involving directivity effects have been identified for the largest induced Oklahoma earthquakes (López-Comino and Cesca, 2018; Lui and Huang, 2019). A common pattern reflecting rupture propagation toward or away from injection wells is difficult to establish, also due to the variety in rupture styles. The 2011 Mw 5.7 Prague and 2016 Mw 5.0 Cushing earthquakes ruptured away from the injection wells, whereas the 2016 Mw 5.1 Fairview earthquake ruptured toward the injection. Lui and Huang (2019) attributed the difference in rupture directions to expected pressurization of the fault zone, which relates to the distance away from injection zones and total injected volume.

Induced seismicity in Oklahoma provides a unique opportunity to systematically compare the migration direction of each seismic cluster with respect to injection well locations. Each cluster will be characterized by a so-called migration vector calculated using an enhanced migration technique based on previous work (Haffener et al., 2018). Seismicity occurs in a region with many high-rate disposal wells and high-pressure perturbations causing difficulties to establish appropriate associations among earthquakes and wells. In this context, we introduce a new methodology to calculate a so-called well vector associated to multiple injection wells. Finally, we explore plausible lateral migration patterns depending on different parameters such as the distance from injection wells, injected volumes weightings and equivalent magnitude of each cluster.

2 Data

We use a relocated earthquake catalog, recorded between 2010 and 2016, with enhanced spatial resolution, a magnitude of completeness (M_c) of 2.5, and a minimum magnitude of 2.0 (Chen, 2016). We consider individual clusters with at least 20 events identified by Haffener et al., (2018). This resulted in 60 clusters after aftershocks were removed using the space-time windowing method proposed by Uhrhammer (1986) to avoid the space-time imprint of aftershocks. The injection data used in this study are obtained from Oklahoma Corporation Commission websites with monthly data from 1995 to 2017 with a total number of 876 disposal wells. Considering maximum well distances of 50 km, the number of injection wells involved in this study is 836 (Figure 1).

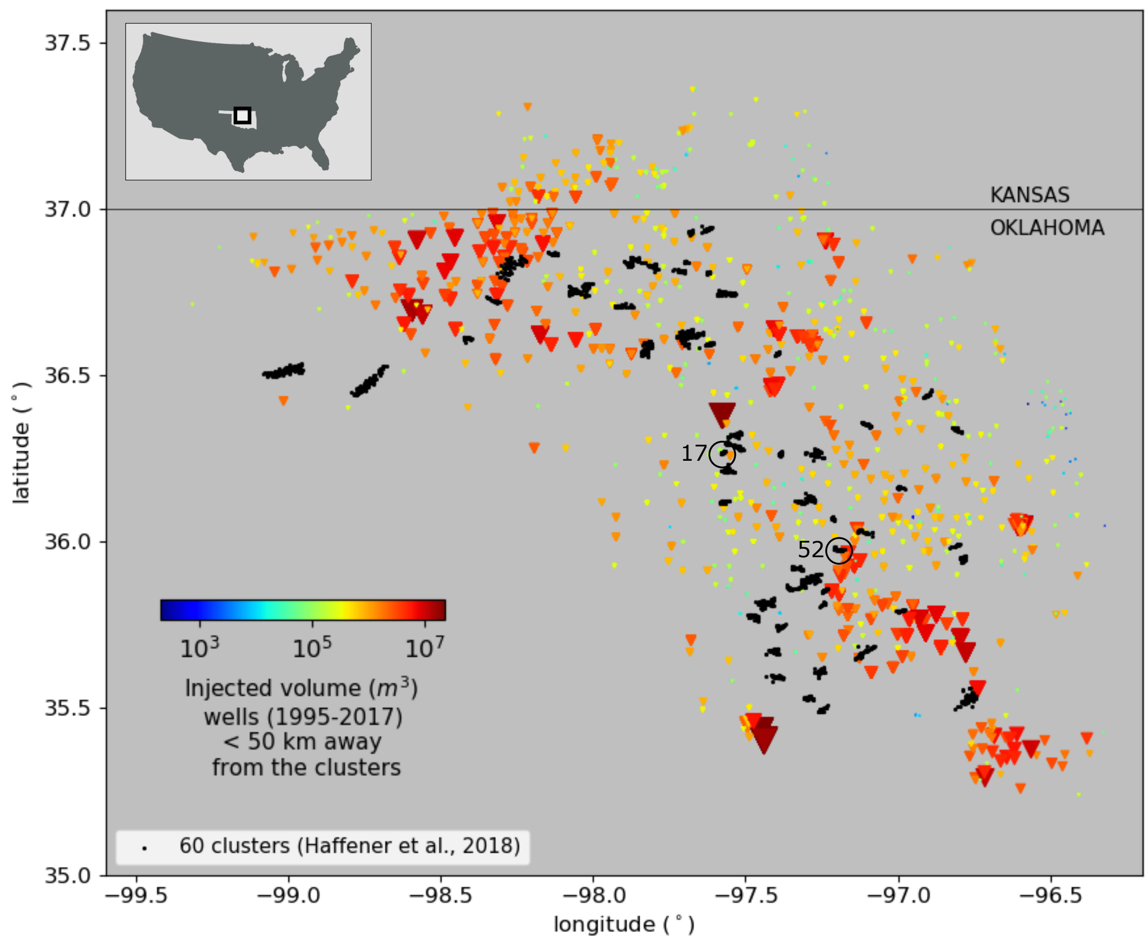

Figure 1. Map of wells (inverted triangles) within a radius of 50 km from the average location in each cluster and 60 seismic clusters in Oklahoma (black dots) detected by a nearest-neighbor approach after aftershocks were removed using a space-time windowing method (Haffener et al., 2018). Wells are scaled (color and size) according to the total injected volume between 1995 – 2017. Two selected clusters (17 and 52) analyzed in Figure 2 and S1 are indicated.

3 Comprehensive migration analysis with respect to multiple injection wells

In our study, we propose a comprehensive migration analysis based on previous approaches involving different numbers of temporal bins of equal duration spanning the period of the entire sequence (Haffener et al., 2018) (Figure 2 and S1). Earthquakes in each cluster are divided into 10 temporal bins (Figure 2a). A spatial bin point is calculated by averaging epicentral locations in each bin, delineating the migration line of each cluster (Figure 2b).

Next, we define the migration vector ($\overrightarrow{v_m}$), as the direction from the 1st spatial bin point to the averaged location of the remaining spatial bin points. Each cluster is then characterized by the azimuth Φ and length r of the migration vector (Figure S2). The notation Φ_0 and r_0 indicates that all events in each cluster were used to calculate the azimuth and length (Figure 2b). To assess uncertainties associated with the calculation of the migration vector, we applied a bootstrap analysis. For each cluster, we calculated 100 migration vectors, randomly removing 10% of events in each repetition (Figure S3). The final Φ and r are then defined from the average locations of the heads and tails of all migration vectors (Figure 2c). We define the associated uncertainties as $\varepsilon_\Phi = \Delta\Phi/2$, where $\Delta\Phi$ is the maximum difference of azimuths calculated from the bootstrap analysis, and ε_r as the standard deviation of r. Significant changes of Φ between repetitions indicate that the cluster does not have a prevailing direction of migration (Figure S1). Therefore, we only consider clusters with $\Delta\Phi < 45°$ in further analysis. Based on this criterion, the migration vectors for 24 clusters were excluded (Figure S4).

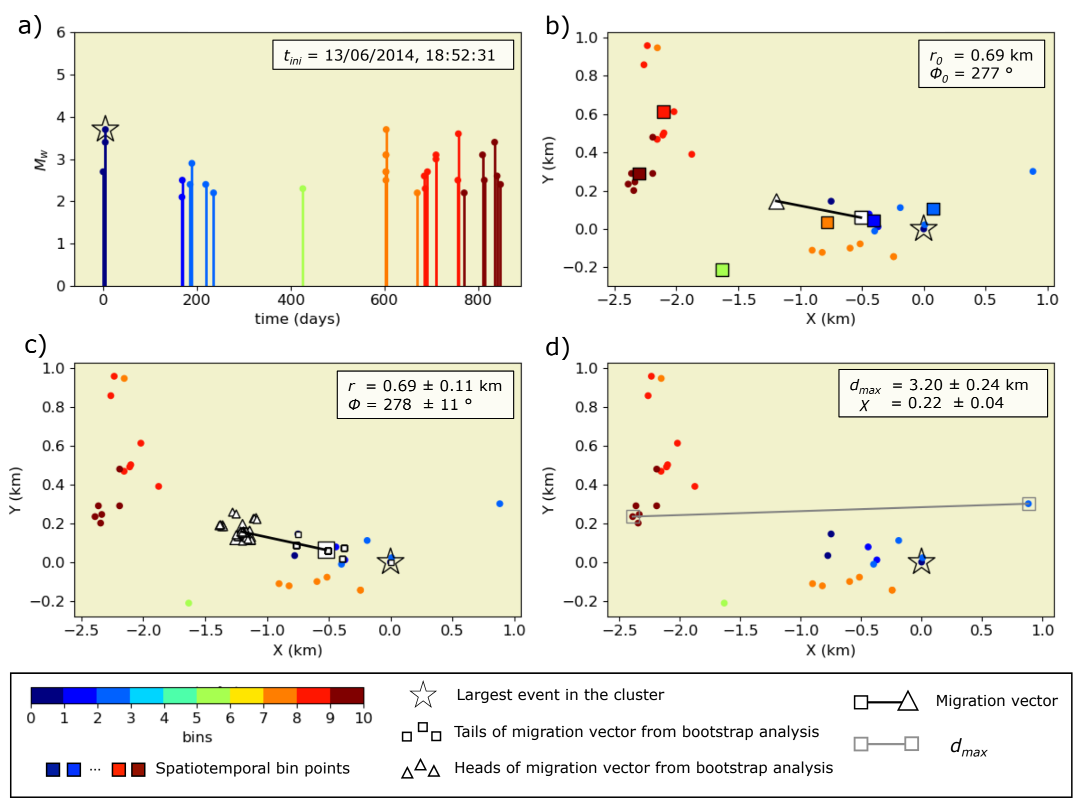

Figure 2. Migration analysis for cluster 52 (see Figure 1) showing results for a stable migration vector. a) Temporal evolution of the seismic sequence from t_{ini}; the color scale indicates association of seismic events with temporal bins and the star depicts the largest event in the cluster. b) The migration vector (black line) defined from tail (white square) to head (white triangle) and the spatiotemporal evolution of migration (color-coded squares indicate the spatiotemporal bin points). r_0 and Φ_0 represent the length and azimuth of the migration vector calculated using all events in the cluster. c) Bootstrap analysis to calculate the final length r and azimuth Φ of the migration vector and their uncertainties. Small white triangles and small white squares depict the heads and tails of 100 migration vectors for the bootstrap analysis. The final migration vector is depicted by a black line from the tail (large white square) to the head (large white triangle). d) The maximum cluster length (d_{max}) and the migration coefficient (χ) are shown with the uncertainties obtained from the bootstrap analysis. d_{max} (gray line), is defined by the two seismic events farthest from each other (open gray squares).

Individual clusters are divided into two groups, according to their spatial migration behavior: migration and non-migration groups, or here so-called strong or weak migration groups. Some authors obtain a statistical significance (s_m) ranging from 0.5 to 1.0 to identify each migration group according a fixed threshold value around 0.8 – 0.85 (Chen et al., 2012). Using such criteria, Oklahoma clusters reveal almost a parity division with around 40 – 50 % clusters belonging to group with strong migration (Haffener et al., 2018). We propose a simple way to quantify this property by calculating the ratio of the length of the migration vector (r) to the maximum length of the cluster (d_{max}) (Figure 2d):

$$\chi = \frac{r}{d_{max}} \qquad \text{(Eq.1)}$$

The migration coefficient (χ) increases from 0 (no migration) to 1 (strong migration), reaching the maximum value only in the case of migration from one end of the cluster to the other. Uncertainties for χ-values are calculated using the bootstrap analysis. A similar distribution for χ is obtained using different bins to calculate the migration vector where a value of 0.2 yields similar results as using s_m to establish the separation among different migration groups (Figure S5).

The association of seismic clusters to specific wells is crucial for determining whether clusters migrate toward or away from the fluid-injection point. Multiple injection points and the long history of injection volumes in Oklahoma complicate the individual associations for each cluster. Similar areas in Alberta (Canada) had addressed this issue through spatiotemporal association filters, discarding wells potentially not associated with earthquake clusters based on a set of association criteria, for instance, epicenters of all temporally associated earthquakes must be within 5 km of the well pad surface location (Schultz et al., 2018).

Here, we propose a new methodology representing multiple injection wells around each cluster using a well vector ($\overrightarrow{\boldsymbol{v_w}}$) defined as the vector from the 1st spatial bin point of the cluster (used previously to define the migration vector) to an injection midpoint (Figure 3). The well vector is also characterized by the azimuth Φ_w and length r_w (Figure S2). The injection midpoint is determined as the weighted centroid of locations of wells, taking into account the spatial and temporal distribution of the volume of injected fluids into individual wells and the expansion of the diffusion front. Injected fluids can be associated with a cluster only if they have sufficient time to reach the location of the cluster. Considering a linear diffusion model, we approximate this time by the diffusion front (Shapiro et al., 2005)

$$\boldsymbol{t_D = \frac{d^2}{4\pi D}}, \qquad \text{(Eq.2)}$$

where D is diffusion coefficient and d is the distance between the well and cluster. For the analysis, we use a representative value for the diffusion coefficient for Oklahoma area (D = 1.5 m^2/s, Haffener et al., 2018). This corresponds, for example, to a delay time t_D for the diffusion front of about 18 months for a well that is located at 30 km from a cluster (Figure S6). To account for the effects of diffusion, a well is associated with a cluster only if the fluid-injection started more than t_D ago. Next, at each time instant t of the seismic sequence, the weight of an individual well j is adjusted according to reported cumulative injected volume $V_j(t-t_D)$ and the injection rate volume $\Delta V_j(t-t_D)$. Note that we consider ΔV as the volume injected each month and therefore t increases in steps of 30 days, consistently with the reporting period of injected volumes. Finally, the individual weights are adjusted to account for the expansion of the diffusion front such as a geometrical spreading effect. Assuming dominantly horizontal diffusion, we consider 2D geometrical spreading, which leads to the weights in the forms of $V_j(t-t_D)/d_j$ and $\Delta V_j(t-t_D)/d_j$. To avoid singularities, we consider d = 1 km for wells with d < 1 km.

Following this procedure, we obtain one injection midpoint for each considered time instant t and their average location then defines the final injection midpoint based on weights from cumulative injected volume and injection rate volumes, respectively. The procedure for cluster 52 is illustrated in Figure 3 for cumulative injected volume and in Fig. S7 for injection rate volumes. We also define the associated uncertainties as $\varepsilon_{\Phi w} = \Delta\Phi_w/2$, where $\Delta\Phi_w$ is the maximum difference of azimuths of individual well vectors, and ε_{rw} is the standard deviation of r_w. Like for the migration vector, also here cases with $\Delta\Phi_w > 45°$ are considered unstable. Using this criterion, we found 36 stable cases when using the cumulative injected-volume weighting and 22 when using the injection-rate volume weighting (Figure S4). A summary of all calculated parameters is shown in the Table S1.

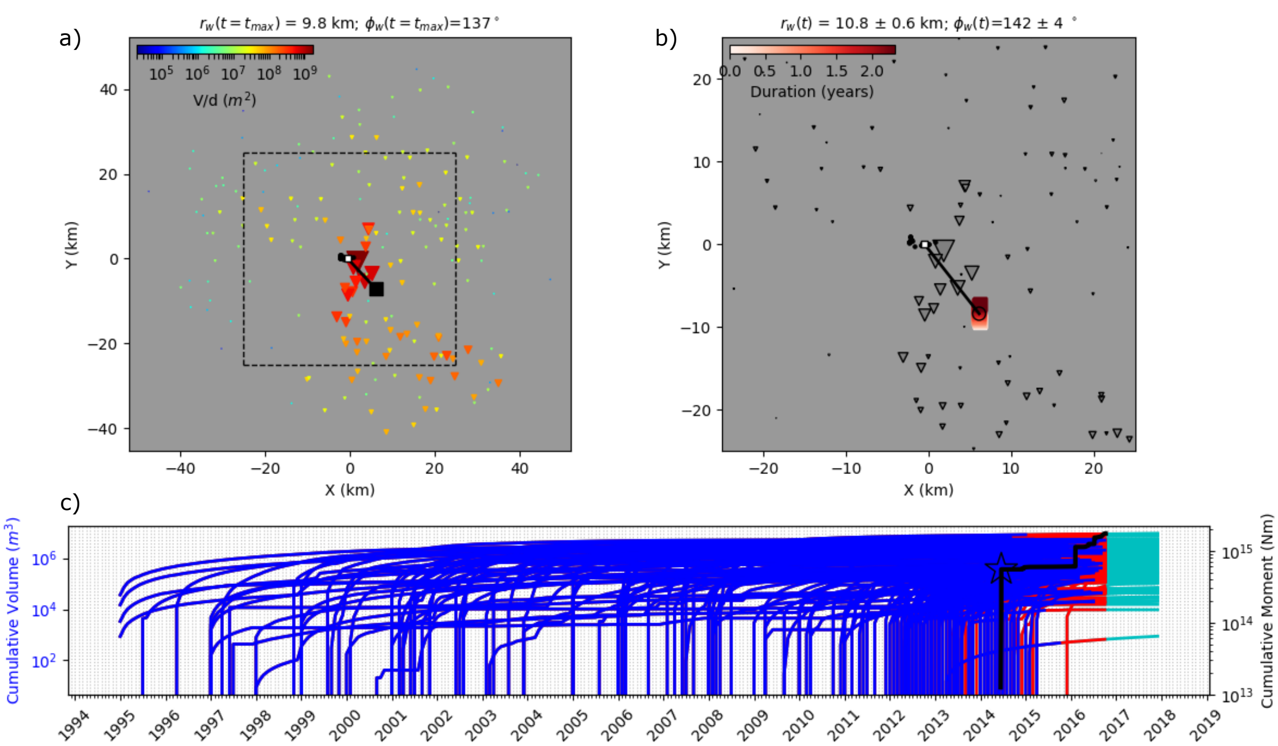

Figure 3. Calculating the well vector for cluster 52 considering the cumulative injected volume weighting. a) Situation at the final time of the seismic sequence t_{max}. The well vector (black line) is defined from the tail of the migration vector (white square defined in Fig 2c) to the injection midpoint (black square). Length (r_w) and azimuth (Φ_w) of the well vector are indicated in the figure header. Wells (inverted triangles) are scaled (color and size) according $V(t_{max}-t_D)/d$. b) Location of injection midpoints during the seismic sequence (color-coded squares). The final injection midpoint is shown with an open black circle, the final well vector by the black line.

Wells are scaled in size as in a). Only the dashed rectangle from a) is shown. c) Cumulative injected volume for the wells associated with the cluster (blue lines) and cumulative seismic moment for the seismic sequence (black line; the largest event is indicated by the star). Red lines indicate the volume that did not affect the cluster due to diffusion constraints, cyan lines indicate data available after the end of seismic sequence.

4 Results

To summarize our results of the comprehensive migration analysis considering multiple injection wells, we define the direction toward or away from injection wells by a parameter κ that represents the angle between the migration vector and the well vector:

$$\boldsymbol{\kappa} = \angle(\overrightarrow{\boldsymbol{v_m}}, \overrightarrow{\boldsymbol{v_w}}). \qquad \text{(Eq. 3)}$$

κ-values range from 0° to 180°, with κ-values closer to 0° indicating an alignment among the migration vector and the well vector for a migration direction toward the injection wells. κ-values closer to 180° indicate the opposite behavior, i.e., migration away from injection wells. We note that the migration vector is also affected by fault geometry as it is most likely oriented along the fault strike. For this reason, we define $\kappa < 60°$ as migration toward wells and $\kappa > 120°$ as migration away. For intermediate cases ($60° < \kappa < 120°$) the migration and well vectors are close to perpendicular, making these cluster a less appropriate choice to decide whether seismicity migrates toward or away from the wells.

In Figure 4 we compare κ as a function of: i) length of the well vector, ii) the total weights assigned to the multiple associated wells based on cumulative injected volumes and injection rate volumes, and iii) the equivalent magnitude (sum of the seismic moments of the events in a cluster expressed as moment magnitude following Hanks and Kanamori, 1979). For this comparison and following analysis, we only consider clusters with strong migration ($\chi > 0.2$): 25 of 36 clusters for the cumulative volume weighting (Figure 4a) and 14 of 22 clusters for the injection rate volume weighting (Figure 4b). Average values and their errors are calculated for clusters migrating toward and away from the wells in order to identify potential lateral migration patterns. Depending on r_w, larger differences among these average toward (13 and 16 km) or away (8 and 10 km) values are observed for both weightings. However, no significant changes are appreciated depending on the weighted volumes and the equivalent magnitude. Additionally, the histograms of κ-values for cumulative injected-volume weighting indicate that a small majority of clusters (60%) documents a migration away from the wells (Fig 4a4).

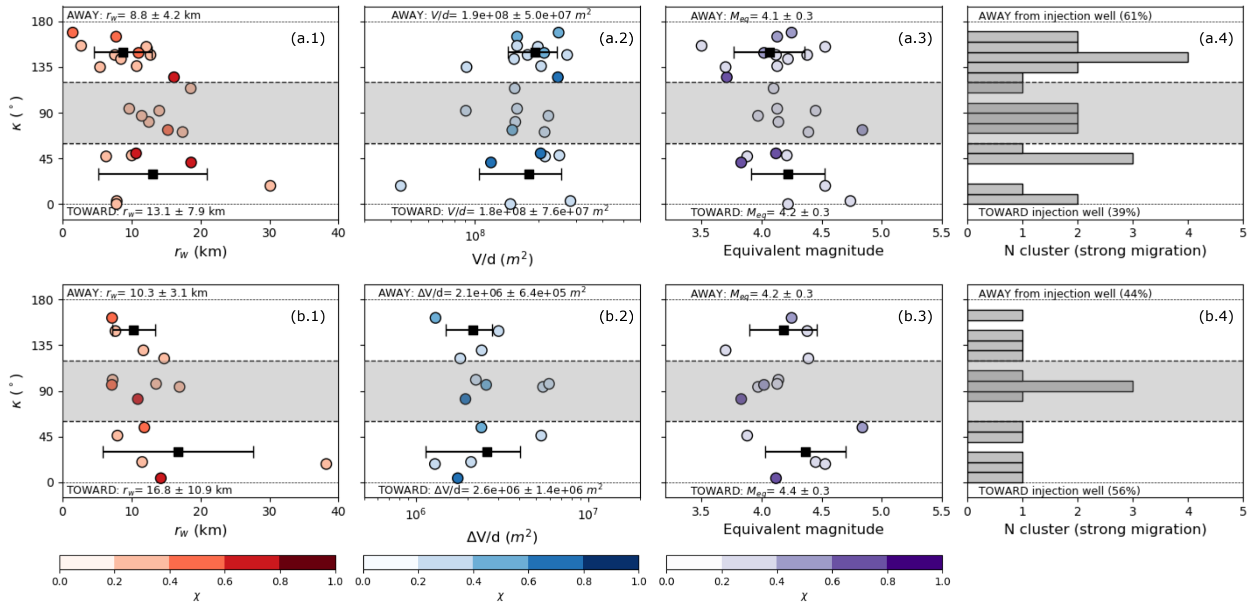

Figure 4. Lateral migration patterns toward or away from injection wells characterized by κ-values using 10 temporal bins in the comprehensive migration analysis (for diffusion coefficient of 1.5 m^2/s). κ-values for strong migration clusters ($\chi > 0.2$) are plotted as circles scaled in color according the migration coefficient (χ), considering the cumulative volume weighting (a) and the injection rate volume weighting (b). Results are shown for each cluster according to the length of the well vector (a.1 and b.1), the total weights assigned to the multiple associated wells in relation to cumulative injected volumes and injection rate volumes (a.2 and b.2) and the equivalent magnitude (a.3 and b.3). Average values and error bars (black squares and lines) are indicated for propagation toward (κ < 60°) and away (κ > 120°) from the injection point (see labels). Histograms are also shown including percentages values (a.4 and b.4). Intermediate cases (60° < κ < 120°) are not considered (gray background separated by black dashed lines).

5 Discussion and conclusions

A comprehensive migration analysis is applied to decipher the potential relationship between direction of lateral earthquake migration of induced seismic events and the location of multiple injection wells. We introduced a new parameter, κ, to quantify the direction of lateral migration toward or away from the injection point based on the angle between the migration vector and the well vector. This parameter facilitates the identification of these lateral migration patterns and it can be used to compare results in other fluid-injection stimulated areas.

A representative migration line, obtained by joining spatiotemporal bin points identified for a cluster, yields complex shapes/patterns for clusters with no predominant migration direction or with bilateral migration. To compare results for a large number of clusters, we approximate the trajectory by the migration vector. The migration starting point (generally assumed to be the epicenter of the first recorded seismic event in the cluster) is a relevant parameter to obtain a representative migration vector. However, we consider that the migration starts at the 1st spatial bin point, which more accurately defines the first activated fault area than the location of just the single seismic event. Because the complete spatiotemporal history of the seismic sequence must contribute to defining the head of the migration vector, the average epicentral location of the remaining spatial bin points is used.

We introduced a simple way to quantify the strong/weak migration through a migration coefficient χ, computed from the length of the migration vector and the total length of the cluster. χ-values for all clusters show an asymmetric (positively skewed) distribution with a long tail toward the largest χ-values (Figure S5). A median value of this distribution ($\chi \sim 0.2$) provides similar results as using s_m criterions to divide the Oklahoma clusters into strong/weak migration groups. Clusters with χ-values larger than 0.2 show an observable migration, but below this value the length of the migration vector is too short to observe any predominant migration directions.

We also propose a new strategy to define representative well vectors associated with multiple injection points surrounding a seismic cluster, considering two types of weighting. The cumulative volume weighting may better represent cumulative effects of pore pressure build up from the beginning of the injection, while injection rate volume weighting may better represent effect of pore pressure variations. From an operational point of view, injection rate weighting may vary significantly over a short time scale, which can cause significant changes of the direction of the well vector during the course of the cluster (Figure S7), as documented by 22 identified unstable well vectors. In contrast, the cumulative volume weighting provides more stable results with no unstable well vectors (Figure S4). Also, different directions of the well vector can be found for each weighting in the same cluster (Fig 3b and S7b).

Regardless of the influence of the weighting on well vector orientation, we observe similar patterns when comparing propagation towards (small κ) and away (large κ) from the wells, depending on the r_w (Figure 4a.1 and 4b.1) and the equivalent magnitude (Figure 4a.3 and 4b.3). Significant differences are observed only according to r_w, revealing the cluster-well distances as a key factor to control these processes. Migration away from injection wells is found for distances shorter than 5-13 km, while an opposite migration towards the wells is observed for larger distances. Both distributions overlap, indicating that there is no monocausal relationship with distance, but the general trend is clear. Accordingly, at shorter cluster-well distances where hydraulic connections between faults and injection wells can be involved, the seismicity is triggered by propagating pore-pressure front (Shapiro et al., 2005). The cumulative injected volume weighting provides the most stable results revealing clearly this pattern for cluster with $r_w < 5$ km. For larger distances, the previous assumption becomes questionable. Outside of the high-pressure zone, poroelastically-induced Coulomb-stress-changes should surpass pore pressure changes, providing a plausible triggering mechanism in the far-field of injection wells (Goebel et al., 2017). The transition from pore-pressure dominance to poroelastic stress based on distance could explain the changes in migration pattern at further distances, which is observed for r_w in the range between 5 - 20 km. For $r_w > 20$ km, our only observation corresponds to the Woodward cluster, confirming this behavior.

The observed patterns remain stable for different choices of the diffusion coefficient (D = 1.25 – 1.75 m^2/s, Fig S8 and S9), which further supports robustness of the well vector-based approach. Also, different choices of temporal binning (5, 10, 15 and 20) yield similar and consistent results (Figs S10 and S11). Considering only 2 bins in the injection rate volume weighting, we obtain similar results such as the statistical parameter d_s which assesses the distance separation between the centers of the first half and second half of each cluster (Chen and Shearer, 2011; Chen et al., 2012). Overall, the comparison indicates that 10 bins is a reasonable choice for our study.

Folesky et al. (2016) analyzed the directivity effects of the largest seismic events associated with the stimulation of geothermal reservoir in Basel (Switzerland) and found that the preferred rupture propagation depends on magnitude. They found that events with $M_L > \sim 2$ propagated backward into the perturbed volume while smaller events propagated away from the well. Our analysis, with minimum equivalent magnitudes around 3.5, shows a different situation, with a significant number of clusters migrating away from the injection wells, and no clear dependence on magnitude.

In conclusion, albeit the main migration pattern in Oklahoma reflects a downward migration from the Arbuckle layer to the basement (Schoenball and Ellsworth, 2017b, Haffener et al., 2018), we found clear lateral migration patterns involving the cluster-well distance as the main factor to control preferred migration directions toward or away from the injection wells. While clusters closest to the wells show a predominant migration away from the wells attributed to pore-pressure changes, we also observe an opposite behavior toward the wells for larger distances that could be controlled by poroelastic stress changes.

Acknowledgments

We thank the Oklahoma Geological Survey (OGS) and USGS for continuous monitoring earthquake activities in Oklahoma. The catalogs for earthquake are obtained from OGS (https://www.ou.edu/ogs) and the seismic clusters from Haffener et al., 2018. The disposal well data are obtained from Oklahoma Corporation Commission (OCC). The research presented in this article is supported by King Abdullah University of Science and Technology (KAUST) in Thuwal, Saudi Arabia, by FRAGEN project (Fracture activation in geo-reservoirs - physics of (induced) earthquakes in complex fault networks), URF/1/3389-01-01, BAS/1/1339-01-01, and Spanish project CGL2015-67130-C2-2-R. J.A.L.C has also received funding from the European Union's Horizon 2020 research and innovation programme under the Marie Skłodowska-Curie grant agreement Nº 754446 and UGR Research and Knowledge Transfer Found – Athenea3i; and by the Deutsche Forschungsgemeinschaft (DFG, German Research Foundation) – Projektnummer (407141557). We also thank Justin Rubinstein and Simone Cesca for constructive comments and discussions. We thank two anonymous reviewers and the GRL Associate Editor for invaluable comments that helped to improve this study.

References

Chen, C. (2016). Comprehensive analysis of Oklahoma earthquakes: From earthquake monitoring to 3D tomography and relocation (Phd dissertation), University of Oklahoma.

Chen, X., Shearer, P. M., & Abercrombie, R. (2012). Spatial migration of earthquakes within seismic clusters in Southern California: Evidence for fluid diffusion. Journal of Geophysical Research, 117, B04301. https://doi.org/10.1029/2011JB008973

Cheng, Y., & Chen, X. (2018). Characteristics of seismicity inside and outside the Salton Sea Geothermal Field. Bulletin of the Seismological Society of America, 108, 1877–1888. https://doi.org/10.1785/0120170311

Ellsworth, W. L. (2013). Injection-induced earthquakes. Science, 341, no. 6142, 1–7.

Ester, M., Kriegel, H.-P., Sander, J., & Xu, X. (1996). A density-based algorithm for discovering clusters in large spatial databases with noise. In Proceedings of the 2nd International Conference on Knowledge Discovery and Data Mining (KDD-96). Portland, OR: AAAI Press.

Goebel, T., Weingarten, M., Chen, X., Haffener, J., & Brodsky, E. E. (2017). The 2016 Mw 5.1 Fairview, Oklahoma earthquakes: Evidence for long-range poroelastic triggering at >40 km from fluid disposal wells. Earth and Planetary Science Letters, 472, 50–61. https://doi.org/10.1016/j.epsl.2017.05.011

Folesky, J., J. Kummerow, S. A. Shapiro, M. Häring, and H. Asanuma (2016). Rupture directivity of fluid-induced microseismic events: Observations from an enhanced geothermal system, J. Geophys. Res. 121, no. 11, 8034–8047.

Haffener, J., Chen, X., & Murray, K. (2018). Multiscale analysis of spatiotemporal relationship between injection and seismicity in Oklahoma. Journal of Geophysical Research: Solid Earth, 123. https://doi.org/10.1029/2018JB015512

Hanks, T., and H. Kanamori (1979), A moment magnitude scale, J. Geophys. Res., 84, 2348–2350.

Hincks, T. , Aspinall, W. , Cooke, R. and Gernon, T. (2018). Oklahoma's induced seismicity strongly linked to wastewater injection depth, Science 359 (6381), 1251-1255.

López-Comino, J. A., & Cesca, S. (2018). Source complexity of an injection induced event: The 2016 Mw 5.1 Fairview, Oklahoma earthquake. Geophysical Research Letters, 45, 4025–4032. https://doi.org/10.1029/2018GL077631

Lui, S. K. & Huang, Y. (2019). Do injection□induced earthquakes rupture away from injection wells due to fluid pressure change? Bulletin of the Seismological Society of America, 109(1), 358-371.

Passarelli, L., Rivalta, E., Jónsson, S., Hensch, M., Metzger, S., Jakobsdóttir, S. S., Maccaferri, F., Corbi, F., Dahm, T. (2018): Scaling and spatial complementarity of tectonic earthquake swarms. - Earth and Planetary Science Letters, 482, pp. 62-70. DOI: http://doi.org/10.1016/j.epsl.2017.10.052

Schoenball, M., & Ellsworth, W. L. (2017). Waveform relocated earthquake catalog for Oklahoma and Southern Kansas illuminates the Regional Fault Network. Seismological Research Letters, 88(5), 1252–1258. https://doi.org/10.1785/0220170083

Schoenball, M., & Ellsworth, W. L. (2017b). A systematic assessment of the spatiotemporal evolution of fault activation through induced seismicity in Oklahoma and southern Kansas. Journal of Geophysical Research: Solid Earth, 122, 10,189–10,206.

Schultz, R., Atkinson, G., Eaton, D. W., Gu, Y. J. & Kao, H. (2018). Hydraulic fracturing volume is associated with induced earthquake productivity in the Duvernay play, Science 359, 6373, 304–308, doi: 10.1126/science.aao0159.

Shapiro, S. A., Rentsch, S., & Rothert, E. (2005). Characterization of hydraulic properties of rocks using probability of fluid-induced microearthquakes. Geophysics, 70(2), F27–F33. https://doi.org/10.1190/1.1897030

Uhrhammer, R. (1986). Characteristics of northern and southern California seismicity. Earthquake Notes, 57(1), 21.

Vidale, J. E., and P. M. Shearer (2006), A survey of 71 earthquake bursts across southern California: Exploring the role of pore fluid pressure fluctuations and aseismic slip as drivers, J. Geophys. Res., 111, B05312, doi:10.1029/2005JB004034.

Wang, Y., G. Ouillon, J. Woessner, D. Sornette, S. Husen (2013). Automatic reconstruction of fault networks from seismicity catalogs including location uncertainty, Journal of Geophysical Research: Solid Earth 118 (11), 5956-5975, doi: 10.1002/2013JB010164,

Weingarten, M., Ge, S., Godt, J., Bekins, B., & Rubinstein, J. (2015). High-rate injection is associated with the increase in U.S. mid-continent seismicity. Science, 348(6241), 1336–1340. https://doi.org/10.1126/science.aab1345

Zaliapin, I., & Ben-Zion, Y. (2013). Earthquake clusters in southern California I: Identification and stability. Journal of Geophysical Research: Solid Earth, 118, 2847–2864. https://doi.org/10.1002/jgrb.50179

AGU PUBLICATIONS

Geophysical Research Letters

Supporting Information for

Lateral migration patterns toward or away from injection wells for earthquake clusters in Oklahoma

J. A. López-Comino[1,2,3,4] M. Galis[5,6], P. M. Mai[1], X. Chen[7] , D. Stich[2,3]

[1] KAUST, King Abdullah University of Science and Technology, Thuwal (Saudi Arabia). [2] Instituto Andaluz de Geofísica, Universidad de Granada, Granada, Spain. [3] Departamento de Física Teórica y del Cosmos, Universidad de Granada, Granada, Spain. [4] Institute of Earth and Environmental Sciences, University of Potsdam, D-14476 Potsdam-Golm, Germany. [5] Faculty of Mathematics, Physics and Informatics, Comenius University in Bratislava, Slovakia. [6] Earth Science Institute, Slovak Academy of Sciences, Bratislava, Slovakia. [7] ConocoPhillips School of Geology and Geophysics, The University of Oklahoma, Norman, OK, USA

Corresponding author: José Ángel López-Comino (jose.lopezcomino@kaust.edu.sa)

Contents of this file

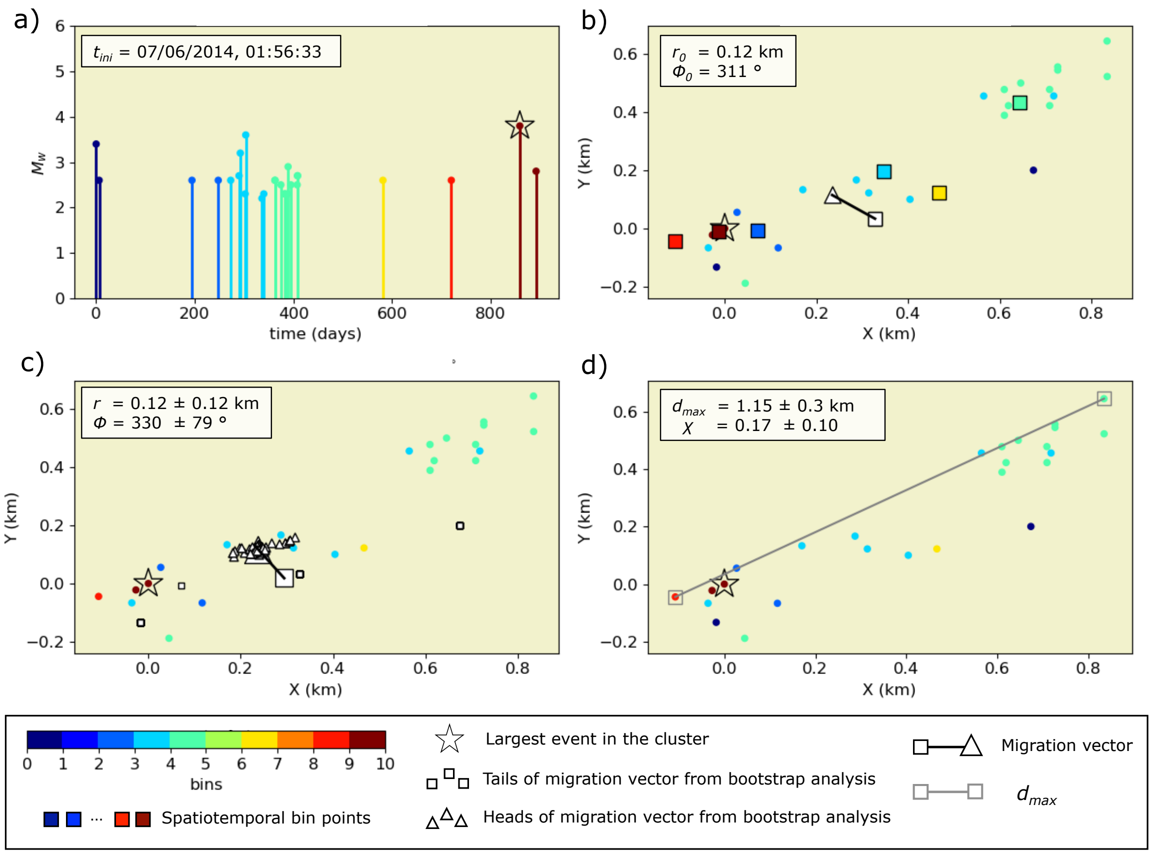

Figure S1. Migration analysis for cluster 17 (see Figure 1) showing results for an unstable migration vector. a) Temporal evolution of the seismic sequence from t_{ini}; the color scale indicates association of seismic events with temporal bins and the star depicts the largest event in the cluster. b) The migration vector (black line) defined from tail (white square) to head (white triangle) and the spatiotemporal evolution of migration (color-coded squares indicate the spatiotemporal bin points). r_0 and $\boldsymbol{\Phi}_0$ represent the length and azimuth of the migration vector calculated using all events in the cluster. c) Bootstrap analysis to calculate the final length r and azimuth $\boldsymbol{\Phi}$ of the migration vector and their uncertainties. Small white triangles and small white squares depict the heads and tails of 100 migration vectors for the bootstrap analysis. The final migration vector is depicted by a black line from the tail (large white square) to the head (large white triangle). d) The maximum cluster length (d_{max}) and the migration coefficient (χ) are shown with the uncertainties obtained from the bootstrap analysis. d_{max} (gray line) is defined by the two seismic events farthest from each other (open gray squares).

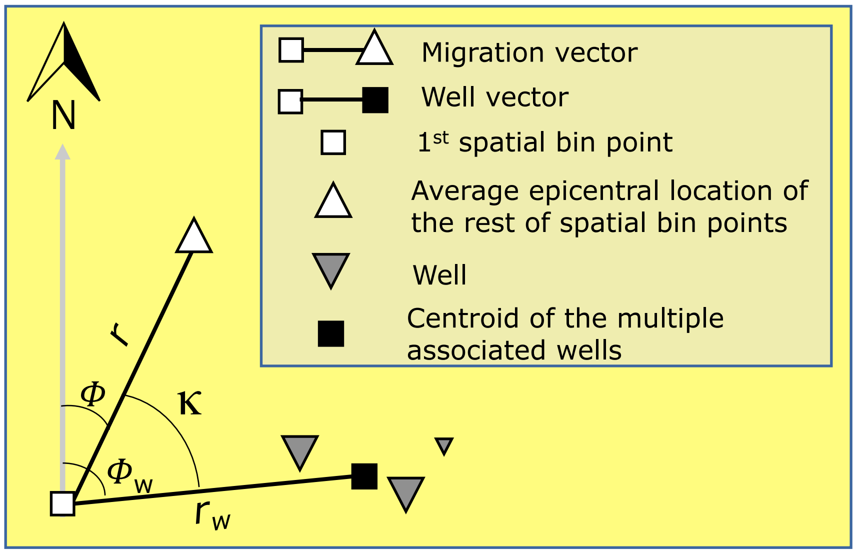

Figure S2. Sketch showing the parameters for calculating the migration and well vector for the comprehensive migration analysis with respect to multiple wells.

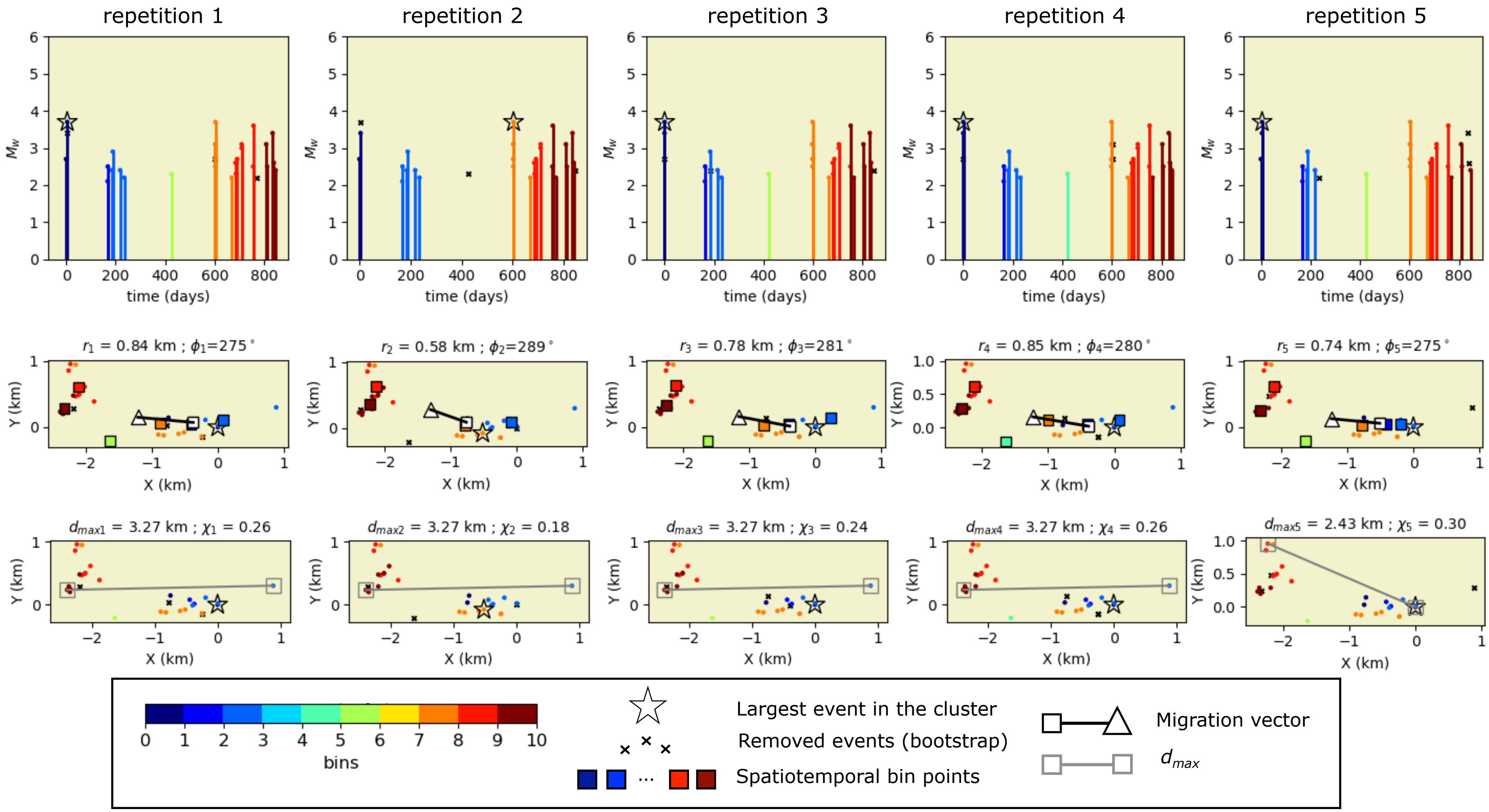

Figure S3. Bootstrap analysis for 5 repetitions (repetitions per columns) to calculate migration parameters for cluster 52. This procedure is repeated 100 times randomly removing the 10% of the events (black x-points). (First row) Temporal evolution of the seismic sequence for each repetition; the color scale indicates different temporal bins associated for each seismic event and the star shows the largest event in the cluster. (Second row) The migration vector (black line) defined from tail (white square) to head (white triangle) and the spatiotemporal evolution of migration (color-coded squares indicate the spatiotemporal bin points). r_i and Φ_i represent the length and azimuth of the migration vector for each *i* repetition. (Third row) The total length (d_{max}) of the cluster (gray line) is defined by the two seismic events farthest from each other (open gray squares) and the migration coefficient (χ) is also shown for each repetition.

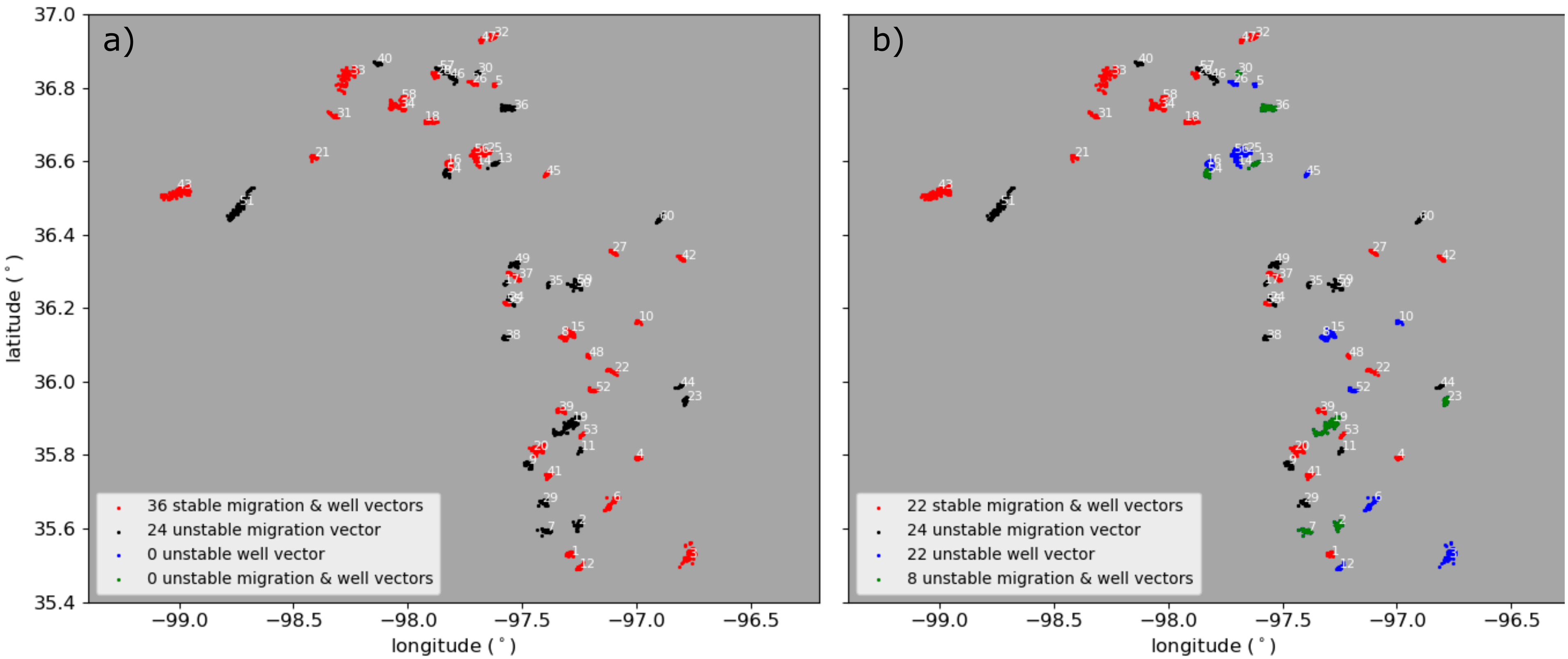

Figure S4. Migration and well vector stability for each cluster (color-coded dots) considering a cumulative volume weighting (a) and an injection rate volume weighting (b). White numbers denote each cluster (see table S1).

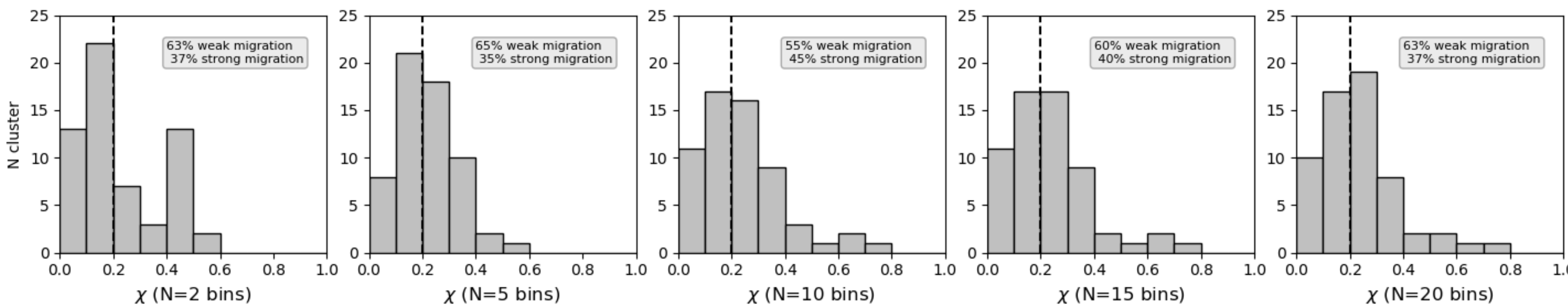

Figure S5. Histograms for the migration coefficient (χ) using different temporal bins (N) in the comprehensive migration analysis. The dashed black lines separates weak ($\chi < 0.2$) and strong ($\chi > 0.2$) migration clusters.

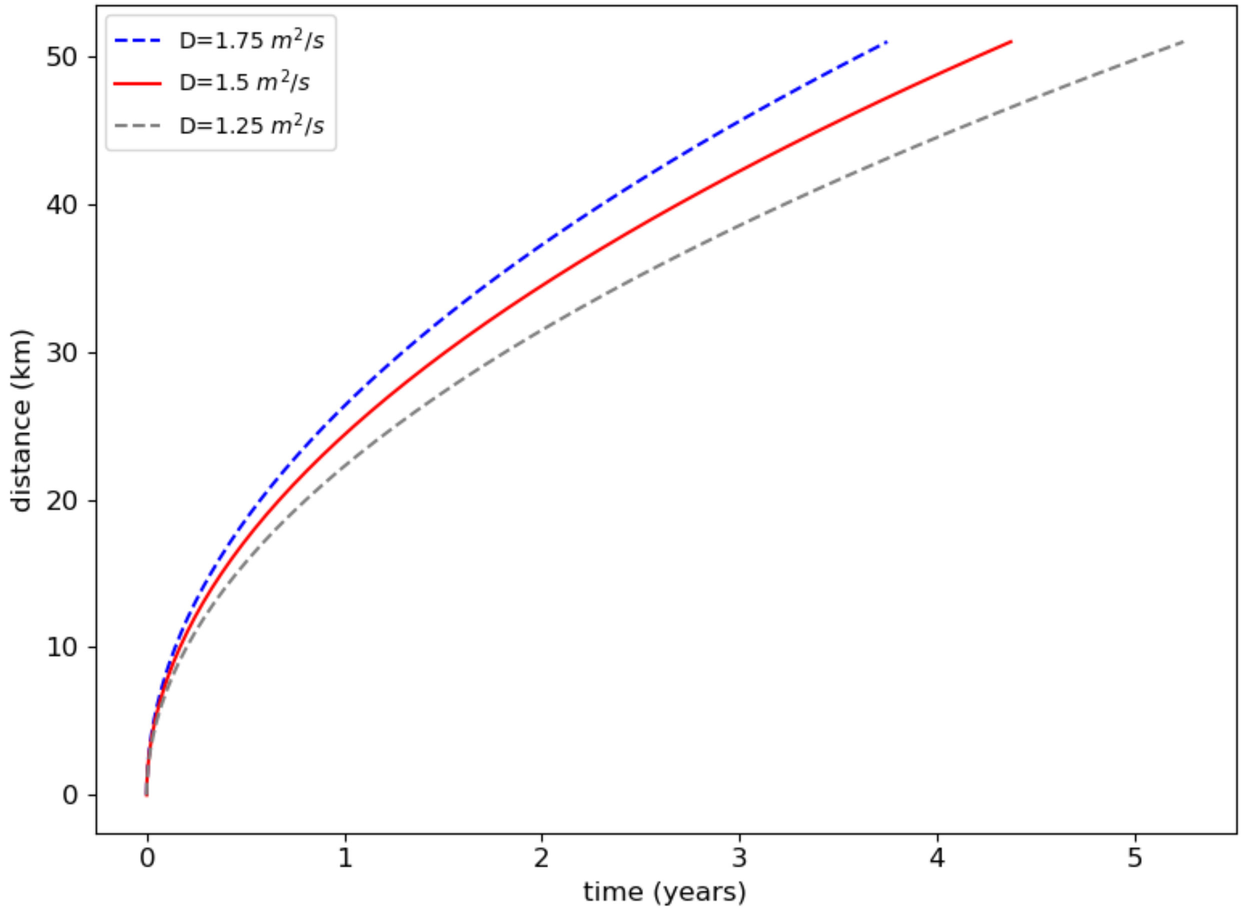

Figure S6. Diffusion fronts according Shapiro et al., 2005 for different diffusion coefficients (D) tested in the comprehensive migration analysis with respect to multiple injection wells.

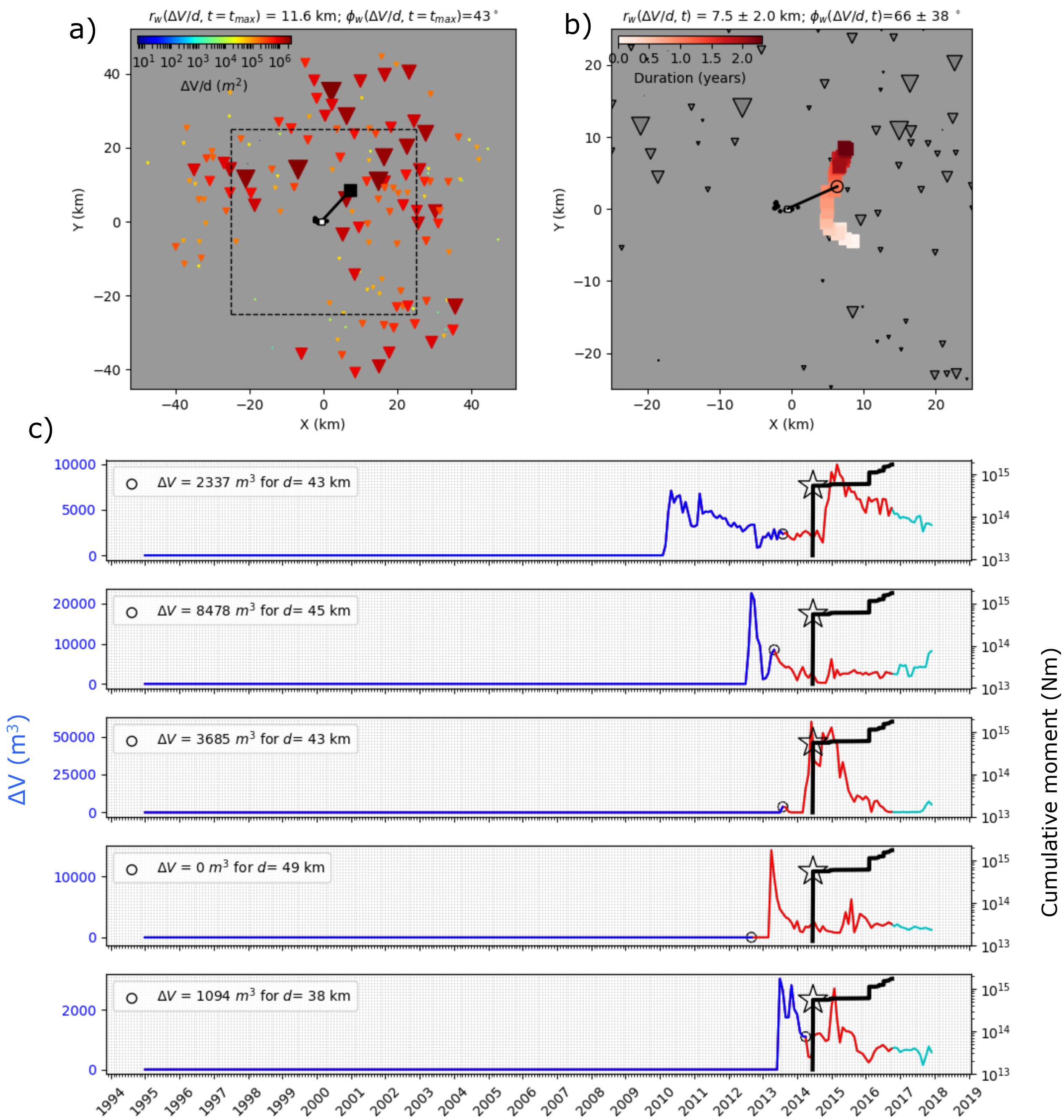

Figure S7. Calculating the well vector for cluster 52 considering the injection rate volume weighting and a diffusion coefficient of 1.5 m^2/s. a) Situation at the final time of the seismic sequence t_{max}. The well vector (black line) is defined from the tail of the migration vector (white square defined in Fig 2c) to the injection midpoint (black square). Length (r_w) and azimuth (Φ_w) of the well vector are indicated in the figure header. Wells (inverted triangles) are scaled (color and size) according $\Delta V(t_{max}\text{-}t_D)/d$. b) Location of injection midpoints during the seismic sequence (color-coded squares). The final injection midpoint is shown with an open black circle, the final well vector by the black line. Wells are scaled in size as in a). Only the dashed rectangle from a) is shown. c) Injection rate volumes for five wells associated with the cluster (blue lines) and cumulative seismic moment for the seismic sequence (black line; the largest event is indicated by the star). Red lines indicate the volume that did not affect the cluster due to diffusion constraints, cyan lines indicate data available after the end of seismic sequence. For each well the injection rate volume (ΔV) with respect to t_{max} (open black circle) and the well distance (d) are indicated.

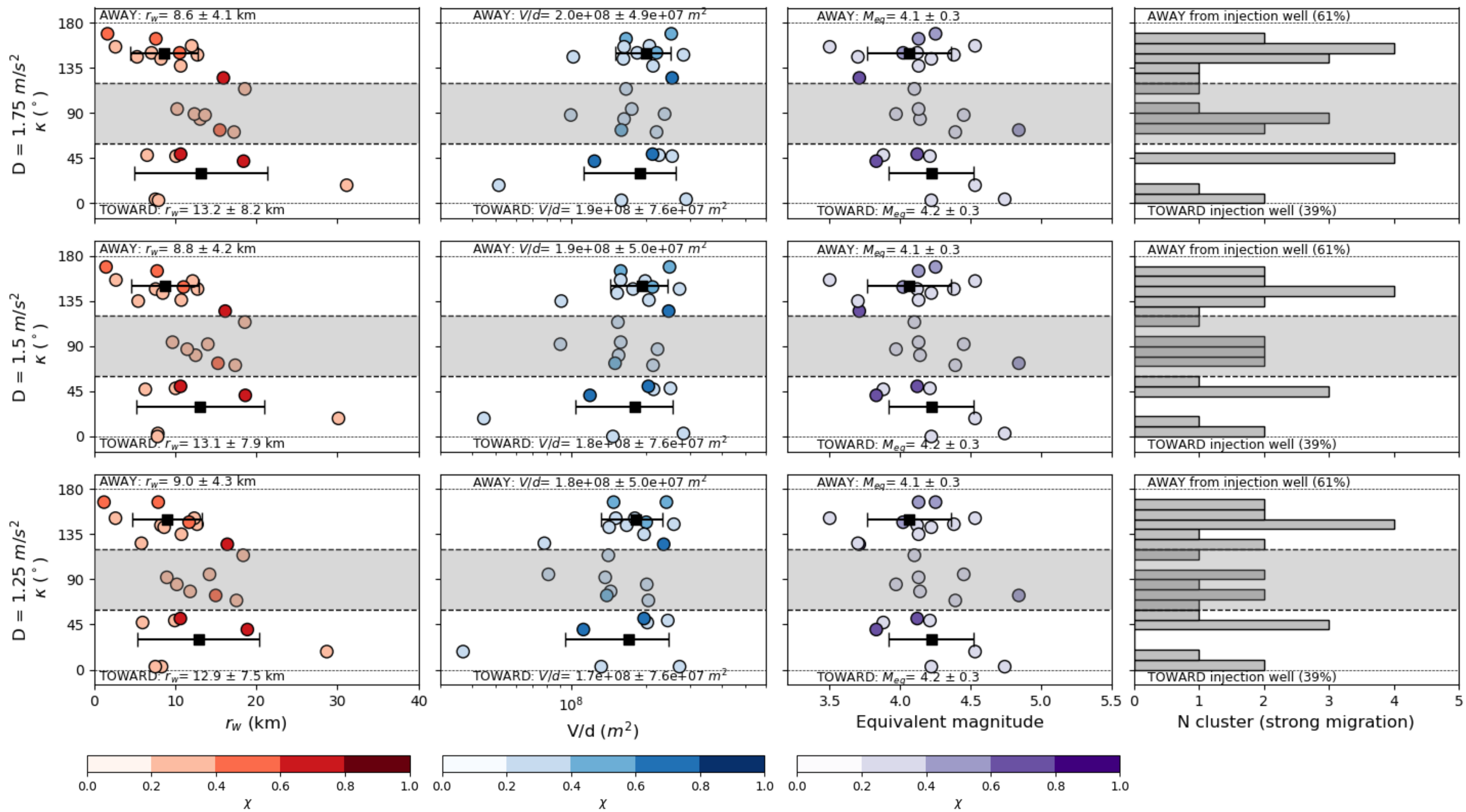

Figure S8. Lateral migration patterns toward or away from injection wells characterized by κ-values using 10 temporal bins in the comprehensive migration analysis and different diffusion coefficients of 1.75 m^2/s (first row), 1.5 m^2/s (second row) and 1.25 m^2/s (third row). κ-values for strong migration clusters (χ > 0.2) are plotted as circles scaled in color according the migration coefficient (χ), considering the cumulative volume weighting. Results are shown for each cluster according to the length of the well vector (first column), the total weights assigned to the multiple associated wells in relation to cumulative injected volumes (second column) and the equivalent magnitude (third column). Average values and error bars (black squares and lines) are indicated for propagation toward (κ < 60°) and away (κ > 120°) from the injection point (see labels). Histograms are also shown including percentages values (forth column). Intermediate cases (60° < κ < 120°) are not considered (gray background separated by black dashed lines).

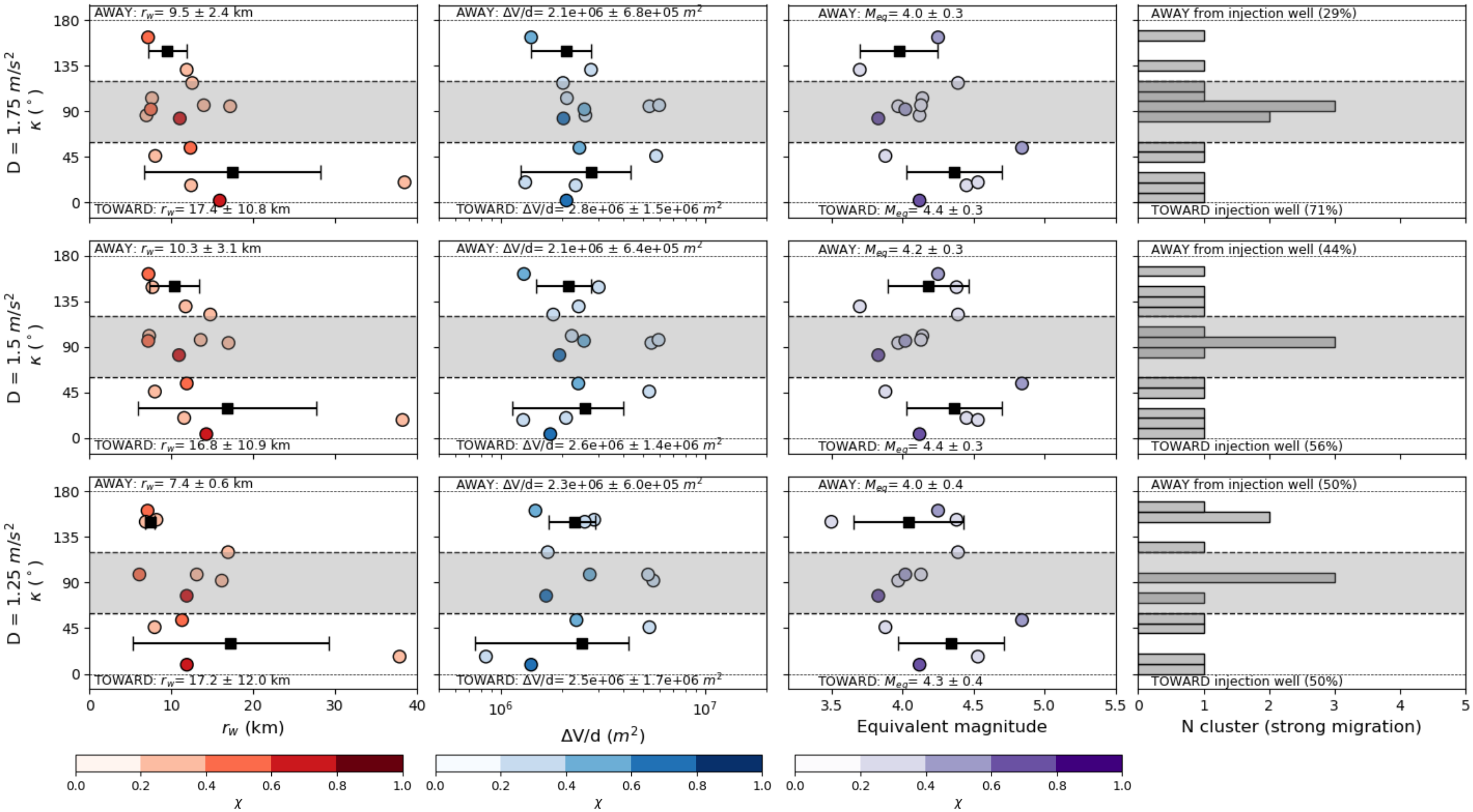

Figure S9. Same as figure S8, but considering injection rate volume weighting. Note that second column show the results according to the total weights assigned to the multiple associated wells in relation to injection rate volumes.

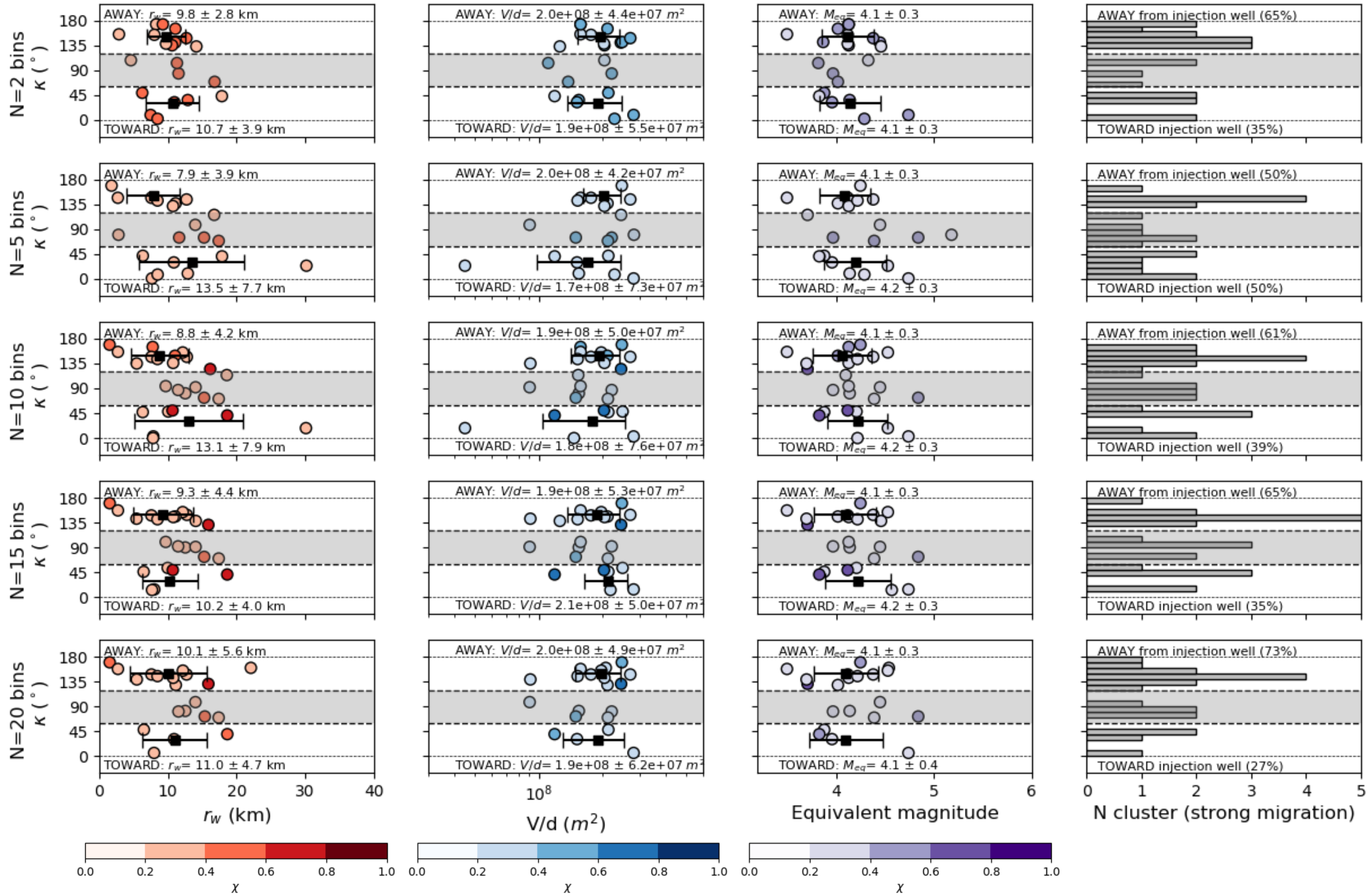

Figure S10. Lateral migration patterns toward or away from injection wells characterized by κ-values using 2 (first row), 5 (second row), 10 (third row), 15 (fourth row) and 20 (fifth row) temporal bins in the comprehensive migration analysis and a coefficient diffusion of 1.5 m^2/s. κ-values for strong migration clusters ($\chi > 0.2$) are plotted as circles scaled in color according the migration coefficient (χ), considering the cumulative volume weighting. Results are shown for each cluster according to the length of the well vector (first column), the total weights assigned to the multiple associated wells in relation to cumulative injected volumes (second column) and the equivalent magnitude (third column). Average values and error bars (black squares and lines) are indicated for propagation toward (κ < 60°) and away (κ > 120°) from the injection point (see labels). Histograms are also shown including percentages values (forth column). Intermediate cases (60° < κ < 120°) are not considered (gray background separated by black dashed lines).

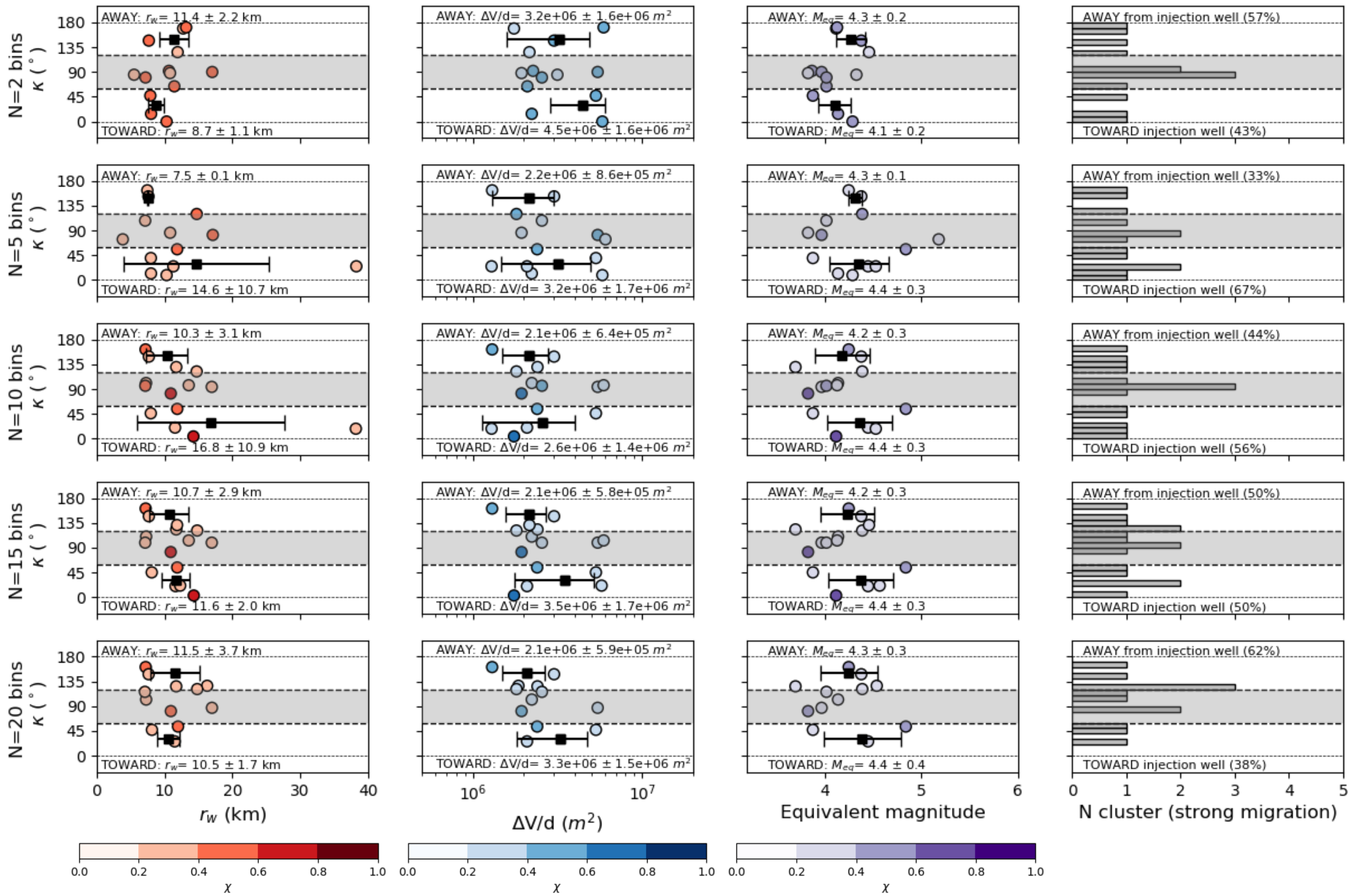

Figure S11. Same as figure S10, but considering injection rate volume weighting. Note that second column show the results according to the total weights assigned to the multiple associated wells in relation to injection rate volumes.

Cluster ID	lon (deg)	lat (deg)	N events	ϕ (deg)	ϕw (deg)		Kappa (deg)		r (km)	dmax (km)	Xi	rw (km)		V/d (m2)	ΔV/d (m2)	Meq (Nm)	Stability (1 = YES & 0 = No)		
																	Migration vector	Well vector	
					for V weighting	for ΔV weighting	for V weighting	for ΔV weighting				for V weighting	for ΔV weighting					for V weighting	for ΔV weighting
1	-97,285	35,528	29	301 ± 9	22 ± 2	42 ± 9	81	101	1,01 ± 0,17	2,74 ± 0,07	0,37 ± 0,06	12,53 ± 0,72	7,27 ± 1,39	1,55E+08	2,23E+06	4,14	1	1	1
2	-97,259	35,613	48	268 ± 37	42 ± 7	116 ± 62	134	152	0,62 ± 0,18	3,52 ± 0,05	0,18 ± 0,05	11,1 ± 1,78	3,87 ± 1,87	2,45E+08	1,76E+06	4,45	0	1	0
3 (Prague)	-96,772	35,522	90	22 ± 17	328 ± 11	93 ± 89	54	71	0,64 ± 0,12	8,36 ± 0,38	0,08 ± 0,01	2,13 ± 0,44	2,18 ± 1,30	2,44E+08	1,16E+06	5,74	1	1	0
4	-97,001	35,792	25	251 ± 3	60 ± 15	89 ± 19	169	162	1,11 ± 0,07	2,50 ± 0,10	0,44 ± 0,04	1,49 ± 0,29	7,19 ± 0,95	2,48E+08	1,30E+06	4,25	1	1	1
5	-97,62	36,809	30	21 ± 18	135 ± 3	137 ± 44	114	116	0,25 ± 0,04	1,06 ± 0,02	0,24 ± 0,03	18,59 ± 3,15	10,72 ± 4,11	1,54E+08	2,52E+06	4,1	1	1	0
6	-97,104	35,675	36	37 ± 10	40 ± 3	158 ± 57	3	121	1,61 ± 0,14	7,10 ± 0,12	0,23 ± 0,02	7,87 ± 0,89	3,38 ± 0,80	2,82E+08	1,74E+06	4,74	1	1	0
7	-97,393	35,593	90	287 ± 39	86 ± 7	154 ± 25	159	133	0,24 ± 0,08	5,07 ± 0,50	0,05 ± 0,01	9,41 ± 0,59	8,65 ± 1,20	2,24E+08	1,10E+06	4,96	0	1	0
8	-97,33	36,124	20	112 ± 14	139 ± 4	24 ± 70	27	88	0,54 ± 0,12	3,07 ± 0,17	0,18 ± 0,05	10,85 ± 1,45	3,55 ± 2,63	1,52E+08	2,40E+06	3,96	1	1	0
9	-97,475	35,775	53	152 ± 67	109 ± 3	140 ± 13	43	12	0,23 ± 0,07	3,34 ± 0,09	0,07 ± 0,02	22,82 ± 0,82	16,84 ± 4,42	2,08E+08	1,86E+06	4,54	0	1	1
10	-96,992	36,165	23	291 ± 11	166 ± 0	160 ± 53	125	131	1,56 ± 0,27	2,19 ± 0,14	0,71 ± 0,10	16,17 ± 1,96	2,10 ± 0,66	2,46E+08	2,53E+06	3,71	1	1	0
11	-97,243	35,814	23	265 ± 26	108 ± 3	156 ± 17	157	109	0,28 ± 0,05	1,78 ± 0,15	0,16 ± 0,02	9,93 ± 0,17	10,63 ± 4,11	2,49E+08	2,27E+06	3,87	0	1	1
12	-97,25	35,494	28	60 ± 21	12 ± 2	309 ± 47	48	111	1,04 ± 0,19	3,41 ± 0,18	0,31 ± 0,05	10,05 ± 0,6	3,69 ± 0,57	2,50E+08	1,28E+06	4,21	1	1	0
13	-97,607	36,596	42	255 ± 89	99 ± 5	66 ± 31	156	171	0,42 ± 0,13	4,41 ± 0,60	0,1 ± 0,02	12,21 ± 1,12	6,62 ± 2,66	1,78E+08	3,28E+06	4,58	0	1	0
14	-97,697	36,591	23	298 ± 19	103 ± 3	46 ± 66	165	108	1,11 ± 0,14	2,64 ± 0,19	0,43 ± 0,04	7,78 ± 1,43	1,37 ± 1,26	1,58E+08	2,77E+06	4,13	1	1	0
15	-97,29	36,138	56	294 ± 5	147 ± 10	19 ± 26	147	85	1,27 ± 0,09	3,77 ± 0,32	0,34 ± 0,04	7,6 ± 1,7	6,22 ± 1,76	1,77E+08	2,51E+06	4,12	1	1	0
16	-97,832	36,594	52	99 ± 18	99 ± 6	46 ± 41	0	53	0,87 ± 0,16	3,03 ± 0,05	0,29 ± 0,06	7,83 ± 2,24	2,11 ± 1,29	1,47E+08	3,28E+06	4,22	1	1	0
17	-97,578	36,267	26	321 ± 79	36 ± 3	49 ± 11	80	93	0,12 ± 0,13	1,16 ± 0,03	0,19 ± 0,11	17,24 ± 1,22	11,87 ± 2,86	1,36E+08	2,27E+06	4,03	0	1	1
18	-97,927	36,71	38	257 ± 19	263 ± 12	291 ± 13	6	34	0,91 ± 0,14	5,18 ± 0,08	0,18 ± 0,03	5,78 ± 0,59	10,22 ± 2,03	1,17E+08	4,68E+06	4,78	1	1	1
19	-97,279	35,891	123	197 ± 41	104 ± 2	77 ± 39	93	120	0,36 ± 0,10	10,86 ± 0,03	0,03 ± 0,01	16,73 ± 0,4	13,01 ± 3,84	1,90E+08	1,62E+06	4,81	0	1	0
20 (Guthrie)	-97,452	35,815	157	288 ± 11	114 ± 2	152 ± 9	174	136	0,81 ± 0,12	5,82 ± 0,21	0,14 ± 0,02	20,49 ± 0,8	13,16 ± 3,89	2,04E+08	1,97E+06	4,7	1	1	1
21	-98,411	36,612	21	271 ± 10	358 ± 5	5 ± 3	87	94	0,79 ± 0,07	2,43 ± 0,06	0,32 ± 0,03	11,49 ± 1,47	16,97 ± 1,55	2,22E+08	5,47E+06	3,97	1	1	1
22	-97,1	36,027	29	292 ± 4	145 ± 3	81 ± 21	147	149	1,05 ± 0,33	4,62 ± 0,11	0,23 ± 0,07	12,76 ± 0,64	7,68 ± 0,41	2,72E+08	3,02E+06	4,38	1	1	1
23	-96,784	35,948	33	334 ± 50	228 ± 5	323 ± 37	106	11	0,75 ± 0,12	2,46 ± 0,04	0,31 ± 0,05	5,73 ± 0,46	4,05 ± 1,34	2,99E+08	2,59E+06	4,19	0	1	0
24	-97,56	36,22	20	49 ± 79	50 ± 1	46 ± 7	1	3	0,64 ± 0,12	3,46 ± 0,07	0,2 ± 0,03	17,02 ± 0,79	11,60 ± 2,01	1,38E+08	2,10E+06	4,02	0	1	1
25	-97,657	36,626	89	258 ± 2	103 ± 5	74 ± 33	155	176	1,95 ± 0,13	6,93 ± 0,13	0,28 ± 0,02	12,16 ± 1,49	6,39 ± 3,42	1,98E+08	2,75E+06	4,53	1	1	0
26	-97,72	36,813	47	109 ± 15	140 ± 6	202 ± 68	31	93	0,46 ± 0,12	3,56 ± 0,07	0,13 ± 0,03	10,2 ± 1,32	4,26 ± 2,44	1,86E+08	3,92E+06	4,44	1	1	0
27	-97,112	36,355	32	118 ± 11	289 ± 3	267 ± 13	171	149	0,43 ± 0,13	2,93 ± 0,06	0,15 ± 0,04	10,24 ± 0,69	5,82 ± 0,99	1,82E+08	2,78E+06	4,33	1	1	1
28	-97,879	36,837	53	149 ± 18	265 ± 9	287 ± 7	116	138	0,46 ± 0,04	2,46 ± 0,00	0,19 ± 0,01	8,16 ± 0,61	12,99 ± 1,82	1,15E+08	3,84E+06	4,06	1	1	1
29	-97,412	35,672	63	66 ± 28	97 ± 6	152 ± 19	31	86	0,27 ± 0,13	3,91 ± 0,09	0,07 ± 0,03	14,47 ± 0,62	13,00 ± 2,45	2,26E+08	1,47E+06	4,83	0	1	1
30	-97,697	36,843	20	108 ± 90	143 ± 6	209 ± 69	35	101	0,06 ± 0,04	1,42 ± 0,09	0,06 ± 0,03	10,41 ± 1,12	5,10 ± 2,40	1,72E+08	3,63E+06	3,92	0	1	0
31	-98,313	36,721	24	297 ± 4	344 ± 0	343 ± 4	47	46	1,29 ± 0,18	4,21 ± 0,12	0,31 ± 0,04	6,33 ± 0,23	7,97 ± 0,21	2,14E+08	5,34E+06	3,88	1	1	1
32	-97,625	36,94	52	238 ± 5	146 ± 4	218 ± 14	92	20	0,98 ± 0,09	3,42 ± 0,20	0,29 ± 0,03	14,03 ± 0,59	11,55 ± 0,74	9,06E+07	2,09E+06	4,45	1	1	1
33	-98,251	36,836	76	193 ± 19	307 ± 11	294 ± 11	114	101	1,07 ± 0,43	9,56 ± 0,05	0,11 ± 0,05	2,38 ± 0,18	3,28 ± 0,47	2,83E+08	6,08E+06	5,18	1	1	1
34	-98,038	36,745	98	278 ± 6	290 ± 6	298 ± 6	12	20	1,30 ± 0,07	6,37 ± 0,09	0,2 ± 0,01	7,67 ± 1,14	12,30 ± 1,27	2,19E+08	5,77E+06	4,57	1	1	1
35	-97,391	36,265	27	49 ± 90	26 ± 1	33 ± 17	23	16	0,02 ± 0,07	1,51 ± 0,05	0,05 ± 0,05	8,07 ± 0,1	7,09 ± 0,58	1,74E+08	2,83E+06	3,94	0	1	1
36	-97,538	36,742	95	5 ± 87	129 ± 2	140 ± 34	124	135	0,45 ± 0,05	5,29 ± 0,04	0,1 ± 0,01	16,28 ± 0,93	10,49 ± 1,52	1,76E+08	2,03E+06	4,24	0	1	0
37	-97,522	36,281	130	114 ± 2	41 ± 4	60 ± 12	73	54	2,91 ± 0,19	5,57 ± 0,07	0,52 ± 0,04	15,28 ± 0,93	11,87 ± 2,78	1,50E+08	2,40E+06	4,84	1	1	1
38	-97,575	36,116	22	355 ± 46	83 ± 1	56 ± 7	88	61	0,30 ± 0,08	2,86 ± 0,03	0,11 ± 0,03	15,11 ± 0,45	8,50 ± 0,91	1,08E+08	1,27E+06	4,45	0	1	1
39	-97,341	35,922	36	112 ± 11	111 ± 1	56 ± 19	1	56	0,51 ± 0,13	3,36 ± 0,05	0,15 ± 0,04	19,66 ± 0,38	8,80 ± 1,05	1,66E+08	1,32E+06	4,62	1	1	1
40	-98,135	36,868	23	275 ± 86	277 ± 1	275 ± 3	2	0	0,21 ± 0,09	2,89 ± 0,02	0,08 ± 0,03	8,3 ± 0,28	10,10 ± 0,31	2,29E+08	5,83E+06	4,29	0	1	1
41	-97,394	35,744	52	30 ± 7	101 ± 2	152 ± 13	71	122	1,14 ± 0,06	2,90 ± 0,13	0,39 ± 0,02	17,41 ± 0,26	14,74 ± 2,88	2,13E+08	1,81E+06	4,39	1	1	1
42	-96,805	36,334	20	121 ± 4	162 ± 1	203 ± 3	41	82	1,81 ± 0,09	2,93 ± 0,02	0,62 ± 0,03	18,65 ± 0,45	10,92 ± 0,20	1,19E+08	1,94E+06	3,83	1	1	1
43 (Woodward)	-99,008	36,525	176	65 ± 11	47 ± 1	47 ± 7	18	18	2,57 ± 0,29	11,50 ± 0,13	0,22 ± 0,03	30,13 ± 1,26	38,24 ± 1,07	4,47E+07	1,29E+06	4,53	1	1	1
44 (Cushing)	-96,811	35,988	27	253 ± 84	202 ± 2	310 ± 14	51	57	0,42 ± 0,19	3,23 ± 0,30	0,14 ± 0,05	6,96 ± 0,48	3,15 ± 0,58	3,09E+08	2,47E+06	5,15	0	1	1
45	-97,397	36,564	27	232 ± 10	76 ± 1	21 ± 73	156	149	0,56 ± 0,06	1,89 ± 0,09	0,3 ± 0,04	2,71 ± 0,06	1,63 ± 1,86	1,58E+08	2,08E+06	3,5	1	1	0
46	-97,815	36,828	41	98 ± 29	258 ± 10	275 ± 12	160	177	0,36 ± 0,18	5,37 ± 0,11	0,07 ± 0,03	7,09 ± 0,91	12,17 ± 1,71	1,44E+08	4,66E+06	4,5	0	1	1
47	-97,68	36,928	27	24 ± 13	159 ± 7	254 ± 4	135	130	0,54 ± 0,07	1,49 ± 0,11	0,37 ± 0,03	5,45 ± 0,25	11,73 ± 1,79	9,13E+07	2,41E+06	3,7	1	1	1
48	-97,211	36,069	20	298 ± 9	149 ± 2	34 ± 8	149	96	0,47 ± 0,04	1,17 ± 0,01	0,41 ± 0,03	11,03 ± 0,54	7,16 ± 0,43	2,12E+08	2,56E+06	4,02	1	1	1
49	-97,535	36,324	55	205 ± 67	27 ± 3	50 ± 15	178	155	0,21 ± 0,11	4,25 ± 0,07	0,06 ± 0,02	12,82 ± 0,42	10,21 ± 1,99	1,45E+08	2,48E+06	4,47	0	1	1
50	-97,268	36,259	33	116 ± 89	4 ± 6	28 ± 12	112	88	0,50 ± 0,21	5,66 ± 0,01	0,09 ± 0,04	4,67 ± 0,05	5,50 ± 0,81	2,05E+08	3,16E+06	4,33	0	1	1
51 (Fairview)	-98,738	36,48	148	269 ± 25	19 ± 3	23 ± 6	110	114	1,67 ± 0,23	13,69 ± 0,18	0,12 ± 0,02	24,84 ± 1,19	28,83 ± 1,60	7,43E+07	2,54E+06	5,31	0	1	1
52	-97,183	35,975	30	278 ± 11	142 ± 4	66 ± 38	136	148	0,69 ± 0,11	3,20 ± 0,24	0,22 ± 0,04	10,76 ± 0,58	7,51 ± 1,99	2,05E+08	2,14E+06	4,13	1	1	0
53	-97,234	35,858	21	46 ± 1	96 ± 1	50 ± 6	50	4	1,39 ± 0,09	2,23 ± 0,06	0,63 ± 0,03	10,67 ± 0	14,26 ± 0,56	2,04E+08	1,75E+06	4,12	1	1	1
54	-97,833	36,568	26	72 ± 62	94 ± 5	61 ± 26	22	11	0,88 ± 0,09	2,63 ± 0,14	0,38 ± 0,04	12,29 ± 1,89	6,25 ± 3,71	1,11E+08	2,78E+06	3,82	0	1	0
55	-97,572	36,214	28	275 ± 8	54 ± 1	47 ± 8	139	132	0,39 ± 0,06	1,93 ± 0,05	0,2 ± 0,03	14,07 ± 0,38	11,86 ± 2,72	1,26E+08	2,16E+06	4,46	1	1	1
56	-97,714	36,621	44	269 ± 8	126 ± 3	147 ± 86	143	122	1,55 ± 0,21	5,19 ± 0,04	0,3 ± 0,04	8,48 ± 1,61	1,48 ± 0,97	1,53E+08	2,98E+06	4,22	1	1	0
57	-97,865	36,849	29	108 ± 90	263 ± 13	283 ± 11	155	175	0,35 ± 0,10	2,71 ± 0,10	0,16 ± 0,04	9,1 ± 0,98	13,65 ± 2,37	1,41E+08	4,51E+06	4,11	0	1	1
58	-98,03	36,771	20	192 ± 13	286 ± 1	289 ± 4	94	97	0,74 ± 0,07	3,03 ± 0,11	0,25 ± 0,02	9,68 ± 0,56	13,57 ± 0,47	1,58E+08	5,93E+06	4,13	1	1	1
59	-97,259	36,268	35	106 ± 86	356 ± 18	29 ± 20	110	77	0,52 ± 0,13	2,41 ± 0,12	0,23 ± 0,06	3,72 ± 0,13	5,69 ± 1,76	2,05E+08	3,05E+06	4,12	0	1	1
60	-96,904	36,441	27	212 ± 90	266 ± 1	248 ± 2	54	36	0,94 ± 0,44	3,47 ± 0,13	0,28 ± 0,12	13,87 ± 0,08	16,43 ± 1,00	1,38E+08	2,44E+06	4,15	0	1	1
																Sum stable cases	36	60	38

Table S1. Parameters derived from the comprehensive migration analysis with respect to multiple injection wells for 60 cluster considered in Oklahoma using 10 temporal bins and a diffusion coefficient of 1.5 m^2/s.